

Saeed Moghimi · Gerhard Gayer · Heinz Günther  
Mehdi Shafieefar

## Application of third generation shallow water wave models in a tidal environment

Received: 14 July 2004 / Accepted: 10 December 2004 / Published online: 3 February 2005  
© Springer-Verlag 2005

**Abstract** Wave modeling was performed in the German Bight of the North Sea during November 2002, using the spectral wave models, namely the K-model and Simulating WAVes Nearshore (SWAN), both developed for applications in environments of shallow water depths. These models mainly differ with respect to their dissipation source term expressions and in exclusion or inclusion of nonlinear wave–wave interactions. The K-model uses nonlinear dissipation and bottom dissipation, and neglects quadruplet wave–wave interaction whereas, SWAN includes, besides bottom dissipation, dissipation by white-capping and depth induced wave breaking and triad wave–wave interaction. The boundary spectra were extracted from the WAM model results of a North Sea hindcast of the HIPOCAS project, wind fields, tidal current and water level variations from the results of models used in the Belawatt project. The purpose of this study was to test the performance of both wave models to see whether they were able to predict near-shore wave conditions accurately. The runs were performed with and without tidal current and level variations to determine their effect on the waves. Comparisons of model results with buoy measurements show that taking into account tides and currents improve the spectral shape especially in areas of high current speeds. Whereas SWAN performed better in terms of spectral shape, especially in case of two peaked spectra, the K-model showed better results in terms of integrated parameters.

**Keywords** Shallow water · Wave spectra · Wave modeling · Nonlinear dissipation

---

### 1 Introduction

In the last decade, spectral wave models for open oceans and shelf seas have reached high standards. These so-called third generation models do not prescribe the spectral shape like models of the second generation anymore, but rather solve an energy balance equation for each bin of the spectral parameter space. Recently, research has focused on the spectral wave models for coastal environments, because an understanding of the waves is essential before answering questions related to coastal protection, environmental control and management, and sustainable development. The prediction of sea states is essential for ports, harbors and navigational channels. Furthermore, the knowledge of the sea state is a key to understand coastal dynamic systems, which consist of coupled atmospheric, hydrodynamic, morphological, and biological subsystems.

Following the sophisticated open ocean spectral wave models, such as WAM-cycle4 (Günther et al. 1992), and WAVEWATCH (Tolman 1991; Tolman and Chalikov 1996), research on the spectral models for coastal applications is currently in progress. A high-resolution small-scale version of WAM has been introduced by Luo and Sclavo (1997) and Monbaliu et al. (2000). In this version of WAM, numerical adjustments related to the small spatial scales have been carried out.

Other third generation spectral wave models such as the K-model (Günther and Rosenthal 1995; Schneggenburger et al. 2000), or Simulating WAVes Nearshore (SWAN) (Booij et al. 1999) were especially developed for and used in near-shore, highly variable tidal environments (Ris et al. 1999) or lakes. The performance of these wave models could be improved by taking into account the changing water depths and currents, hydrodynamical models derived benefit from interactions (e.g., radiation stress, wave-induced currents).

---

Responsible Editor: Hans Burchard

S. Moghimi (✉) · M. Shafieefar  
Tarbiat Modarres University, Tehran, Iran  
E-mail: moghimis@modares.ac.ir

G. Gayer · H. Günther  
GKSS Research Center, Institute for Coastal Research,  
Geesthacht, Germany

Wornom et al. (2001, 2002) showed that use of different propagation schemes in near-shore applications may lead to different results. Use of Cartesian wave propagation in WAM produced more accurate near-shore wave predictions as compared to spherical propagation. In addition, use of a nested specific near-shore wave model such as SWAN can improve the results significantly.

Lin et al. (2002) compared two different wave models, the second generation model GLERL (Great Lakes Environmental Research Laboratory) and the SWAN wave model with respect to measurements in Chesapeake Bay. The simulations have been done without including effects of current and water level variations. Wave breaking and Triad wave–wave interaction were activated in SWAN. Comparison of time series showed that both models over-predicted wave heights and under-predicted the peak period.

In this paper, we compare K-model with SWAN, developed at the GKSS research center and Delft University, respectively. Both the models were conceived as phase-averaged spectral wave models for intermediate and shallow water depths. SWAN is very similar to WAM, but includes shallow water source terms such as depth-induced breaking and triad wave–wave interactions. A new feature of the K-model is the consideration of wave energy dissipation by turbulent interaction.

Basic comparisons were carried out in applications with simplified geometries to help explain special features—e.g., the changing of spectral shapes due to nonlinear interaction or nonlinear dissipation—and differences in both the models, which were observed during real simulation runs for the 10-day period (15th–25th) in November 2002, when occasionally pure swell approached shallow coastal waters meeting young sea wind generated by offshore blowing winds.

This study was carried out to compare model applications in highly variable tidal environments in order to gain insight into the effects of currents and water depths and their variations on the waves, and the importance of different physical processes involved.

The structure of this paper is as follows: Sect. 2 covers the tools and methods of investigation and artificial test cases; Sect. 3 describes the set-up of model systems for the November 2002 application in the German Bight; Sect. 4 includes the description of results, statistical analysis, inter-model-comparisons and comparisons with buoy measurements and Sect. 5 concludes the paper.

## 2 Wave models

### 2.1 Description of the K-model and SWAN

The SWAN model (Simulating WAVes Nearshore, Booij et al. 1999) used in this research is a non-stationary version (Cycle 3, version 40.31), released to the public domain in February 2004.

Both K-model and SWAN are discrete spectral wave models solving the wave action balance equation. In the

case of K-model, this is done in wave number space, with the wave vector modulus and direction ( $k, \theta$ ) in polar coordinates as independent variables. SWAN model uses an equivalent notation in frequency-direction space ( $\sigma, \theta$ ).

The wave action density, defined as  $N \equiv E/\sigma$ , is a function of the spectral parameter space variables as well as of locations  $x, y$  and time  $t$ .  $E$  is the wave energy density and  $\sigma$  the intrinsic angular wave frequency, determined by the dispersion relation

$$\sigma^2 = gk \tanh(kh), \quad (1)$$

fulfilling the Doppler-shift equation

$$\omega = \sigma + k \cdot \vec{U}, \quad (2)$$

where  $\vec{U}$  is the current vector and  $\omega$  the absolute angular frequency. In flux form, the balance equation used in the K-model writes

$$\partial_t N + \partial_x \cdot (\dot{x}N) + \partial_k \cdot (\dot{k}N) + \partial_\theta \cdot (\dot{\theta}N) = S(N). \quad (3)$$

The first term on the left side represents the local rate of change; the second term represents spatial propagation; the third and fourth terms represent refraction (by depth and/or current variations).  $S(N)$  summarizes the energy input and dissipation sources of action density, described in the following section (Schneggenburger et al. 2000).

For details of the action balance equation used in the SWAN model, we refer to Booij et al. (1999) and Holthuijsen et al. (2004).

Integrated parameters used throughout this paper are significant wave height  $H_s$ ,

$$H_s = 4\sqrt{E(f, \theta)df d\theta} \quad (4)$$

mean  $T_{m01}$  period calculated by:

$$T_{m01} = E(f, \theta)df d\theta/E(f, \theta)f df d\theta \quad (5)$$

and mean wave direction calculated by:

$$\arctan(E(f, \theta) \sin \theta df d\theta/E(f, \theta) \cos \theta df d\theta). \quad (6)$$

In addition, the SWAN and the K-model differ in their numerical approaches. In the K-model an explicit integration scheme is used, which limits the time step. SWAN uses an implicit upwind scheme without any restriction. However, after performing test runs in a lake (different time steps, non-stationary mode), we have chosen rather low values which gave results (with respect to  $H_s$ ) comparable with those of the K-model. Increasing the time step by a factor of ten produced local differences in the order of 10%.

### 2.2 Physical processes

The conceptual idea of the K-model is to consider only essential physical processes in order to limit the model

complexity. SWAN offers the opportunity to study in detail (in a specific application) the role of each source function and their different formulations by including or excluding them through keywords.

We decided to activate the indicated default method in the SWAN User Manual to be as close as possible to the physics used in the K-model. Because of very shallow waters (e.g., tidal flats hardly covered by water during high tide conditions), triad wave–wave interaction and wave breaking were also activated.

The physical processes considered in K-model and SWAN, in brief, are as follows.

*Linear wind input* The same form of the Philips input source function, based on the version of Cavaleri and Rizzoli (1981), and modified by Tolman (1991), was used by both the models. Due to a misinterpretation of the User Manual, this source function wasn't activated in the SWAN model runs. This led to a slightly reduced initial wave growth in off-shore wind situations.

*Exponential wind input* The K-model used the Snyder wind input (WAMDI group 1988) with modifications to include the effect of wind 'gustiness'. SWAN's default method for exponential wind input was also used in the WAM model (WAM Cycle 3, the WAMDI group 1988) rescaling the Snyder input term in terms of friction velocity.

*White-capping* The white-capping dissipation source term is not included in the K-model. SWAN's default method for taking into account this physical process is based on a pulse-based model proposed by Hasselmann, as adapted by the WAMDI group (1988).

*Nonlinear dissipation* The K-model uses a nonlinear dissipation source function accounting for dissipation by wave–turbulence interaction (Rosenthal 1989) as introduced by Schneggenburger et al. (1997), based on a 1D version by Günther and Rosenthal (1995). SWAN does not use this source term.

*Bottom-interaction dissipation* Both models use the bottom-interaction dissipation function as described in Hasselmann et al. (1973). Besides this default method, SWAN could use two other methods.

*Depth-induced wave breaking* Depth-induced wave breaking is not included explicitly in the K-model. It is simulated by increasing nonlinear energy dissipation with reducing depth. SWAN uses the total dissipation method (i.e., integrated over the spectrum). Thus, wave breaking in a random field can be modeled well with the dissipation of a bore, as described by Battjes and Janssen (1978).

*Nonlinear wave–wave interactions* Quadruplet wave–wave interactions of waves are also not included in the K-model. Schneggenburger et al. (2000) argued that in

small-scale non-uniform systems quadruplet interactions might be neglected because this theory was developed for strictly homogeneous systems, a prerequisite that is definitely violated in coastal areas. Hence, use of numerical parameterization according to this theory can, in certain cases, lead to substantial errors in applications in nonhomogeneous systems. In the absence of a suitable theory and related parameterization, Schneggenburger et al. (2000) decided to neglect nonlinear energy transfer processes in coastal wave modeling and showed that the use of nonlinear dissipation instead could reproduce qualitative features and empirical laws of wave growth.

SWAN uses the quadruplet wave–wave interactions computed with the discrete interaction approximation (DIA) as proposed by Hasselmann et al. (1985). In addition, SWAN proposes triad wave–wave interaction for very shallow coastal regions; a method based on the lumped triad approximation (LTA) of Eldeberky (1996), which is a slightly adapted version of the discrete triad approximation of Eldeberky and Battjes (1995).

### 2.3 Artificial test cases

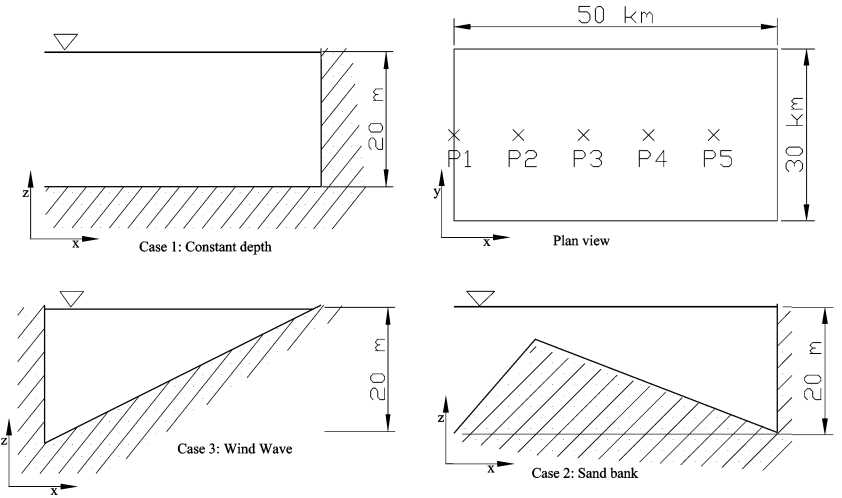
SWAN's model results of the 10-day real simulation period in November 2002 showed an almost permanent underestimation of the  $T_{m01}$  period and sometimes an overestimation of  $H_s$  (during the first 4 days) when compared to those of K-model and measurements. Searching for explanations, we established some artificial test cases in order to get an impression of the behavior of different source terms, especially wave–wave interaction terms. All three test cases are very simplified representations of the real simulation conditions when westerly winds and wave systems prevailed.

Both models were set up on a spatial grid with 1,000 m grid size. The spectral grid consisted of 24 directional bins of  $15^\circ$  and 28 logarithmic scaled frequency (or wave number) bins between 0.01 Hz and 1 Hz ( $0.01\text{--}3.33\text{ m}^{-1}$ ), mapped to an output frequency axis between 0.01 Hz and 1 Hz. For test cases I and II (swell at an open boundary), the input boundary spectrum consisted of energy density components concentrated in the first three frequency bins, each of them initially propagating along the  $x$ -axis. The average frequency (calculated from the first spectral moment) is 0.046 Hz. Total energy input at each boundary point corresponded to a significant wave height  $H_s$  of 2 m. For test case III (fetch dependent wind waves), closed boundaries are assumed.

#### 2.3.1 Case I: swell in constant water depth

In this case, the evolution of a pure swell spectrum in a simple rectangular geometry with constant water depth of 20 m has been studied (Fig. 1).

**Fig. 1** Geometries of different artificial test cases



A change of wave characteristics should be visible due to shallow water effects. After 3 h simulation time the model results of  $H_s$  and  $T_{m01}$  along a longitudinal section are presented in Fig. 2 (left side). SWAN shows a much higher wave height compared to K-model. Quadruplet nonlinear wave-wave interaction causes a sudden decrease in wave period after a distance of 10 km, followed by a gradual increase to a value similar to that of the K-model. Inclusion of the triad nonlinear wave-wave interaction causes an additional decrease in period

of up to 4 s after a distance of 50 km. This can be explained by examining the spectra.

The evolution of the 1D frequency wave spectra at five different points (see Fig. 1) are presented on the right side in Fig. 2. The spectra at the boundary should be identically equal, but a broader spectrum is produced by the K-model because of different spectral 2D interpolations and the transformation from frequency-direction space to wave number-direction space.

**Fig. 2** Swell in constant water depth—comparison of integrated parameters along a longitudinal profile (left panel) and spectra at selected points (right panel)

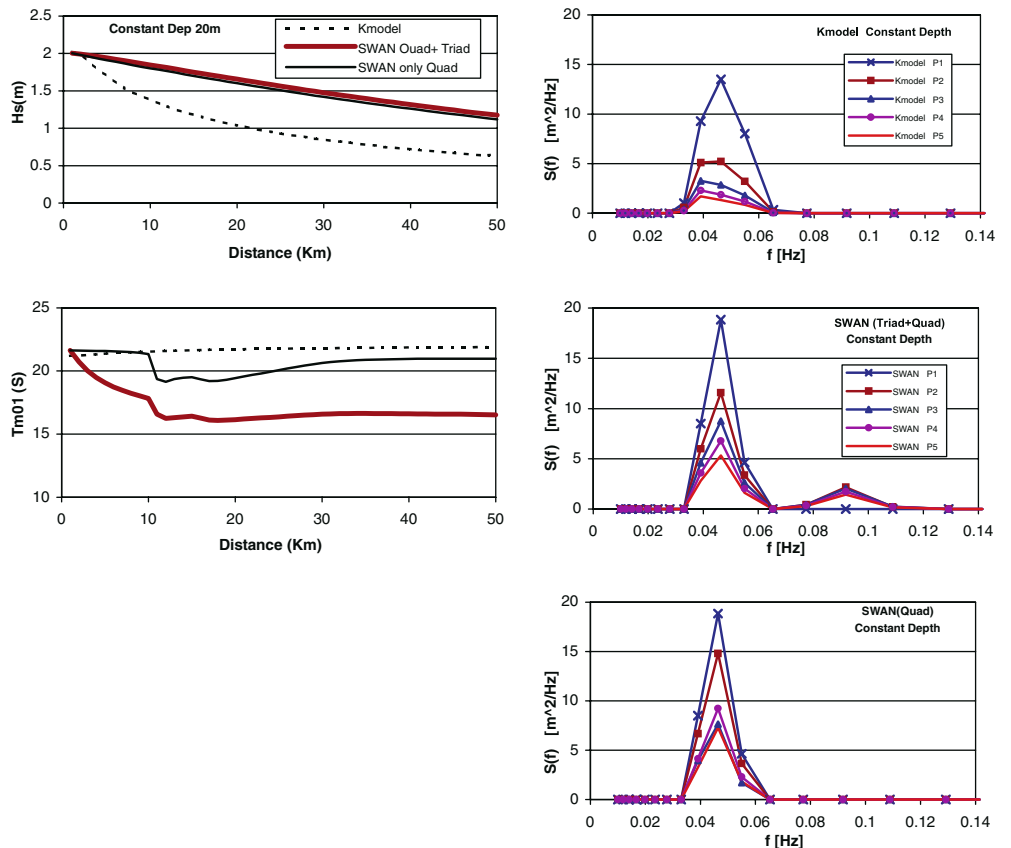
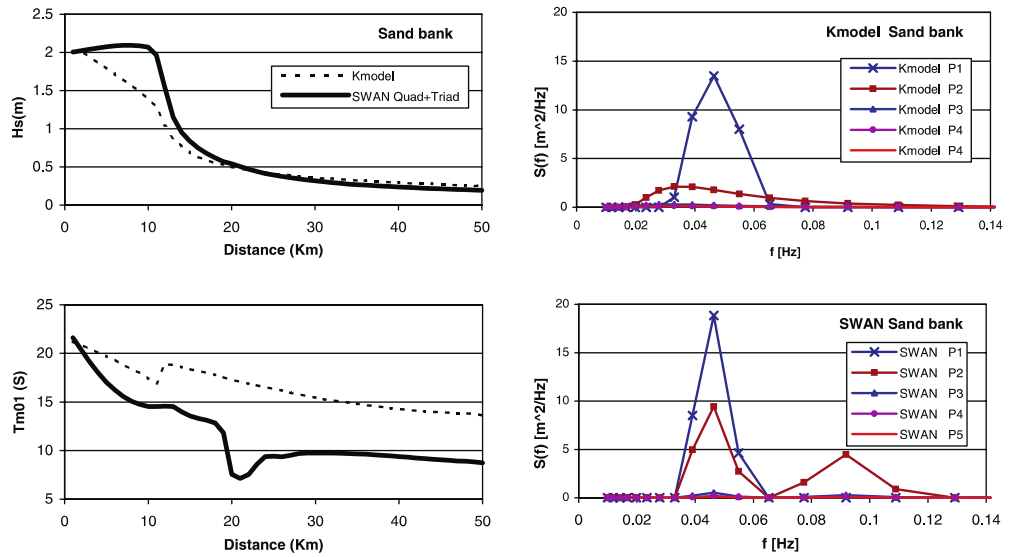


**Fig. 3** Swell over an under water sand bank—comparison of integrated parameters along a longitudinal profile (*left panel*) and spectra at selected points (*right panel*)



SWAN in both cases (including/excluding triad interaction) produces sharp peaked spectra keeping the peak frequency constant during the evolution. In the K-model a shift to lower peak frequencies is observed with the increasing distance from the boundary. An interesting feature is that by including the triad wave-wave interaction in SWAN, a second low energy peak is generated, causing a decrease in  $T_{m01}$  periods.

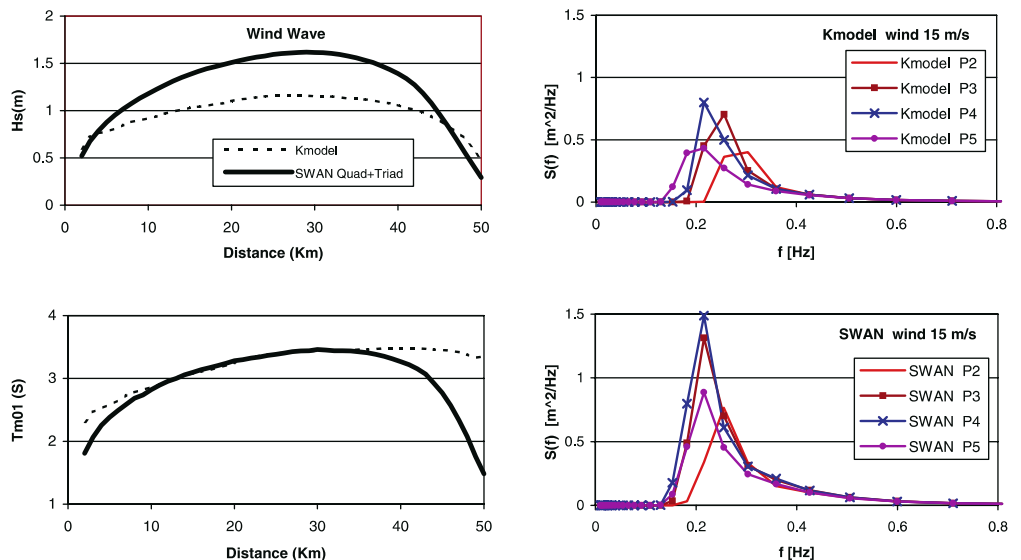
Similar to the real case application, SWAN calculates higher waves and lower  $T_{m01}$  periods (due to triad nonlinear interaction) as compared to the K-model.

effect of varying water depths on  $H_s$  and  $T_{m01}$  along a longitudinal profile and on spectral evolution at selected points is shown in Fig. 3. With respect to significant wave height, the K-model does not show any shoaling effect over the rising bottom slope whereas, this is visible in SWAN.  $T_{m01}$  periods are generally lower in SWAN. The reason of this behavior again can be explained by including triad nonlinear interaction. A second spectral peak is obvious, especially at point (P2) just before the crest of the bank. This was already noticed by Eldeberky (1996). He described that due to nonlinear triad wave interactions and wave breaking frequency spectra developed secondary peaks at harmonics of the peak frequency. Eldeberky also compared this with measured surface elevation spectra taken by Arcilla et al. (1994) showing strong energy transfer to higher harmonics in the shoaling regions.

2.3.2 Case II: swell over an underwater sand bank

This test case is the same as the first one, with respect to the open boundary condition, but instead of constant water depth, here we assume variability in the form of an underwater sand bank (see Fig. 1). The

**Fig. 4** Constant on-shore wind and constant bottom slope—comparison of integrated parameters along a longitudinal profile (*left panel*) and spectra at selected points (*right panel*)



In comparable situations during the real simulations (there are sand banks to the west of the measurement station indicated with H in Fig. 6) we should observe differences in modeled  $T_{m01}$  periods (K-Model's periods are higher than SWAN's).

### 2.3.3 Case III: constant on-shore wind and constant bottom slope

In this case a closed basin with linear decreasing water depths from 20 m to 0 m was used (see Fig. 1). Wind with a speed of 15 m/s was assumed in on-shore direction. The results after 3 h are presented in Fig. 4. With increasing fetch, growing wave heights were observed over the first 30 km, followed by a decrease due to shallow water energy dissipation. Differences in wave heights were quite large. K-model results show an increase in  $H_s$  up to 1.2 m, SWAN reaches a significant wave height of 1.7 m.

The  $T_{m01}$  period calculated by the K-model increases steadily (only near the shoreline we observed; first a slight decrease followed by an increase due to shoaling) whereas, the curve of SWAN shows a strong decrease over the last 10 km. Taking a closer look at the spectra reveals that the peak energies of SWAN are approximately twice as large as those of the K-model with both the models reaching their maximum after 30 km. After P2 SWAN spectra keep the peak frequency fixed, but K-model shows a continuous shift to lower frequencies over the first 30 km.

During the real simulations, in situations when fetch dependent wind waves enter shallow waters, SWAN should give higher waves than K-model. The  $T_{m01}$  periods of SWAN should be lower when closer to the beach.

## 3 Set-up of model systems for the German Bight application

### 3.1 Investigation procedure

Considering the data availability and related ongoing research in the German Bight, the area near the island of Sylt named Hoernum tidal inlet and Hoernum basin was selected for model applications. The main reason for this decision was to investigate the effects of current and water depth variations on wave fields and to study the distribution of wave energy to facilitate the knowledge of sediment mobilization in sediment transport and morphodynamic models.

The area of interest is located in the German Bight in the southeastern part of the North Sea (Fig. 5). For November 2002, wave rider buoy measurements were available at two stations, namely the Hoernum buoy (H in Fig. 6) and the Westerland buoy, further toward the north (W in Fig. 6).

Because both stations are exposed to coastal currents and waves generated in the North Sea, and positioned in

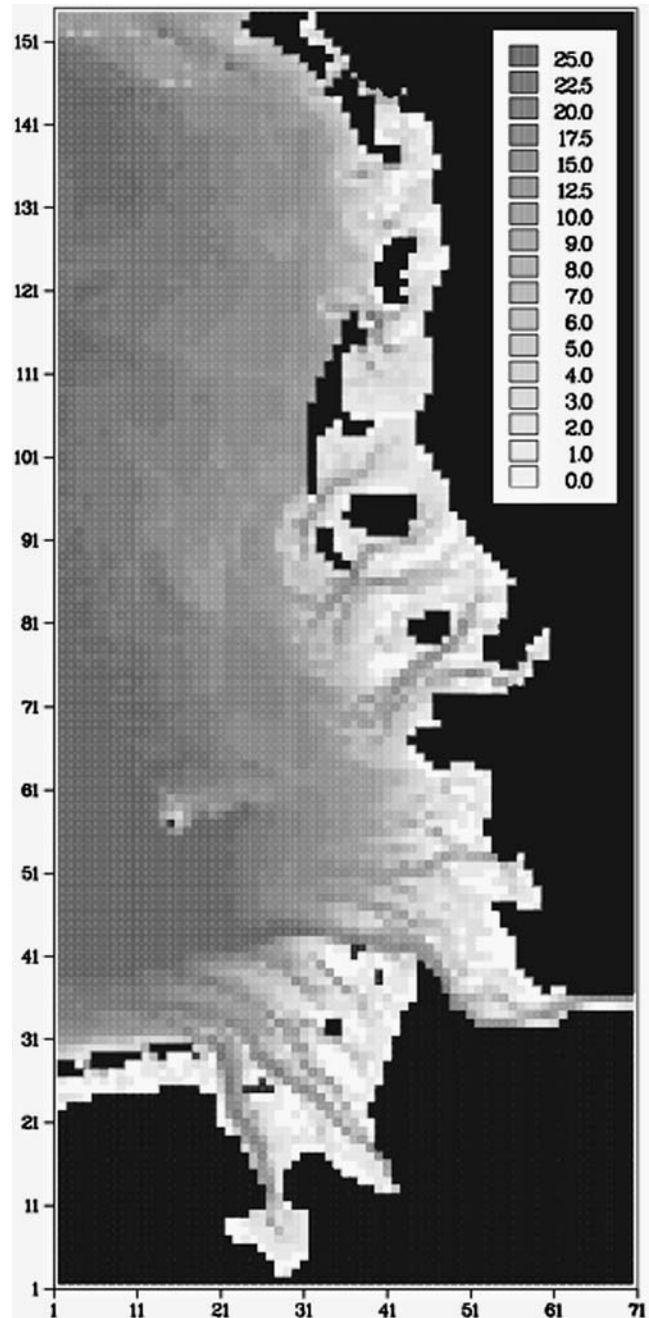
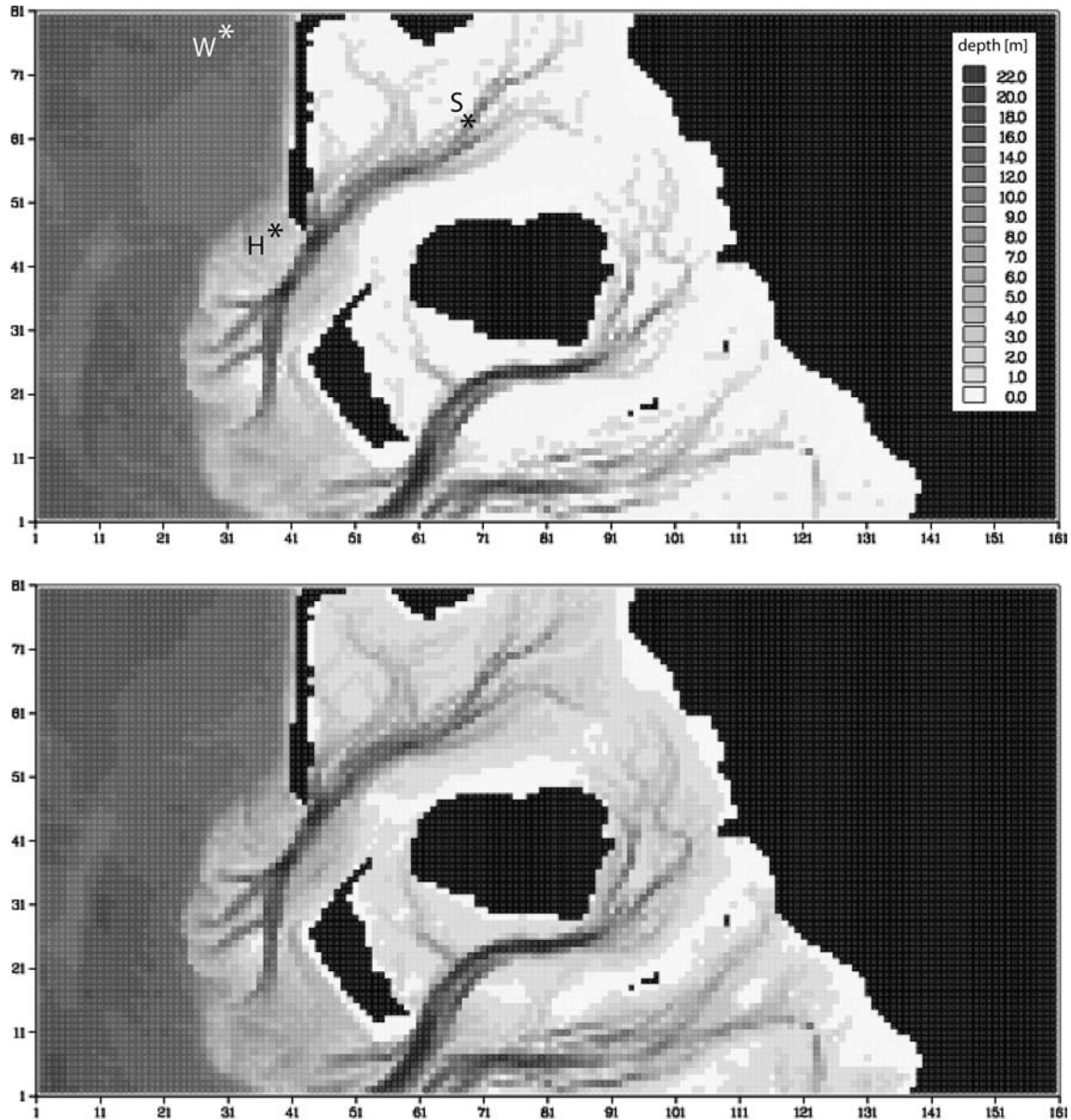


Fig. 5 Coarse grid bathymetry

areas with local high tidal variability, wave modeling had to be performed as part of nested hydrodynamic and wave model systems. Figure 5 shows the bathymetry of the coarse grid with a spatial resolution of 1,600 m; Fig. 6 the bathymetries of the fine grid (400 m resolution) during low tide (upper panel) and high tide (lower panel). On average the range of water level variations is  $\pm 1.5$  m with respect to mean water level. The tidal channel at the inlet at Hoernum has depths between 12 m and 21 m over a width of approximately 2 km. Here the current can reach velocities of up to 1.5 m/s.



**Fig. 6** Fine grid bathymetry during ebb and flood.  $X$  indicates measurement stations

To identify the applicability, reliability and behavior of two third generation spectral shallow water wave models in such environments, a comprehensive analysis and inter-comparisons of model output as well as comparisons with available buoy measurements have been performed.

Input data have been prepared in such a way to generate identical boundary and forcing conditions for both wave models.

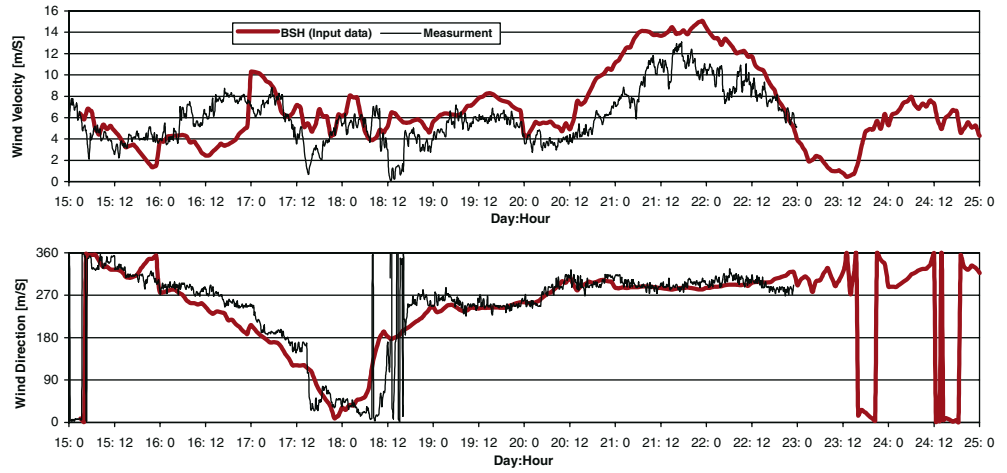
The simulation of tidal current and water level variations in the German Bight have been performed using TRIMPPxyz (Eppel et al. 2003) with boundary and forcing data being provided by the BSH (Federal Maritime and Hydrographical Agency, Hamburg, Germany).

Wave boundary spectra have been extracted from the results of the WAM model established in the HIPOCAS (Hindcast of Dynamic Processes of the Ocean and Coastal Areas of Europe) project (Weisse and Gayer 2000).

### 3.2 Wind field data

Hourly surface wind (at 10-m height above sea surface) and atmospheric pressure fields in the German Bight for November 2002 have been provided by the operational model system of the BSH on a grid with a spatial resolution of 1 nautical mile, based on meteorological forecasts supplied by the DWD (German Weather Service). Time series of input winds of the model grid point corresponding to the buoy location and measured surface winds from a pile closer to the coast during November 2002 are presented in Fig. 7.

**Fig. 7** Measured (*thin lines*) and model input (*thick*) wind velocities (*upper panel*) and directions (*lower panel*) at Westerland. Directions are 'going to', measured clockwise from north



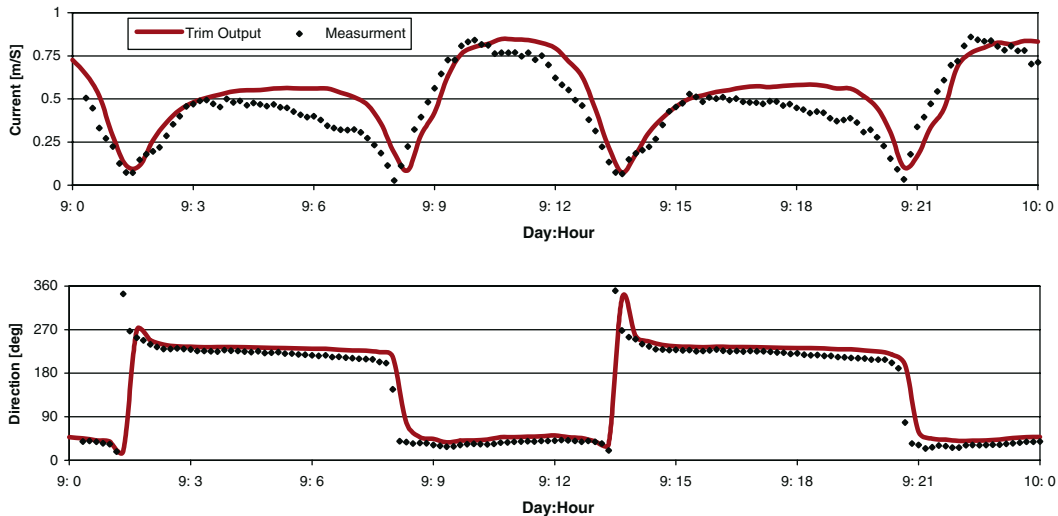
Turning winds occurred during the period between 15th and 19th of November 2002. Whereas the differences in directions ('going to', measured clockwise from geographic North) are moderate in most cases, we often observe greater mismatches in wind speeds. During this period we expect swell from the open North Sea and/or locally generated wind waves with on-shore directions.

During the period of off-shore blowing winds from 19th to 23rd the modeled wind speeds up to 15 m/s are generally higher than the measured wind speeds due to the reduced influence of the land roughness. During this period, fetch dependent wind wave regimes will be dominant, sometimes encountering old swell systems from the North Sea.

### 3.3 Hydrodynamical modeling

To take into account the influence of current and water depth variations on waves, we set up TRIMPPxyz, a

**Fig. 8** Comparison of TRIMPPxyz (*full lines*) current speeds (*upper panel*) and directions (*lower panel*) with ADV measurements (*dotted lines*) during 9th of August 2002 at location S (see Fig. 6). Directions are 'going to', measured clockwise from north



parallel nested version of the hydrodynamic model TRIM (Casulli and Cattani 1994 and Casulli and Cheng 1992).

Currents, water levels, water temperatures and salinity for the initial state and at open boundaries of the coarse grid were taken from the output of the 3D routine circulation model of the BSH. Output fields of water depths and horizontal current velocities of the uppermost layer (initial thickness=2 m) were stored every 30 min to be used as wave model input.

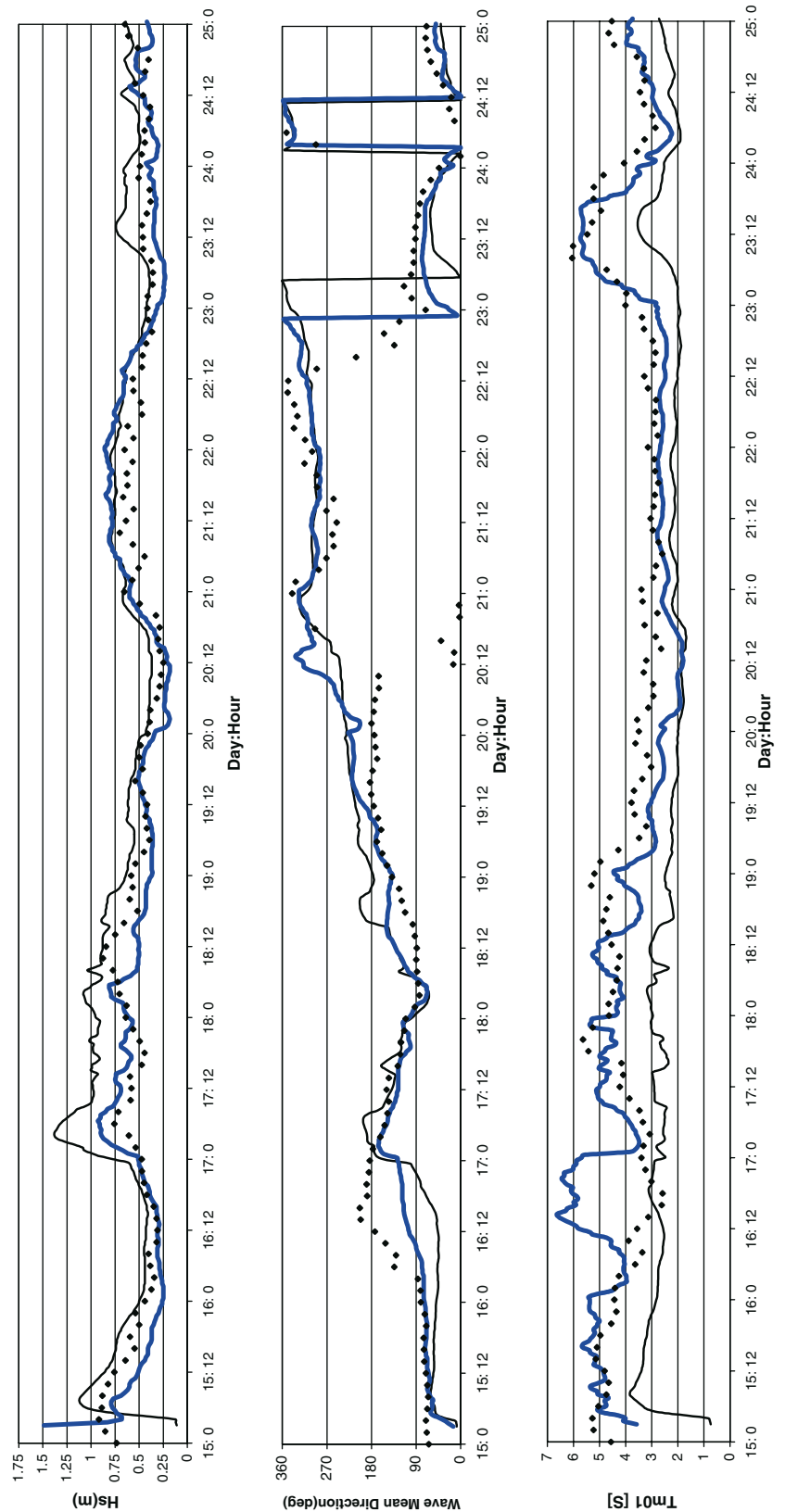
The quality of the current model results could be assessed by comparison with measurements (Fig. 8) in the main channel at the position indicated by S in Fig. 6. The measurements were done by the GKSS research center, on 9th of August 2002, with ADV (Acoustic Doppler Velocity Meter) at a reference depth of 4.3 m. The corresponding model grid point had an initial depth of 4.8 m. The directions compare quite well, whereas modeled current speeds stay too high to the end of flood and ebb tides.

### 3.4 Boundary spectra

The first concern for modeling waves inside the German bight was to provide proper boundary spectra required



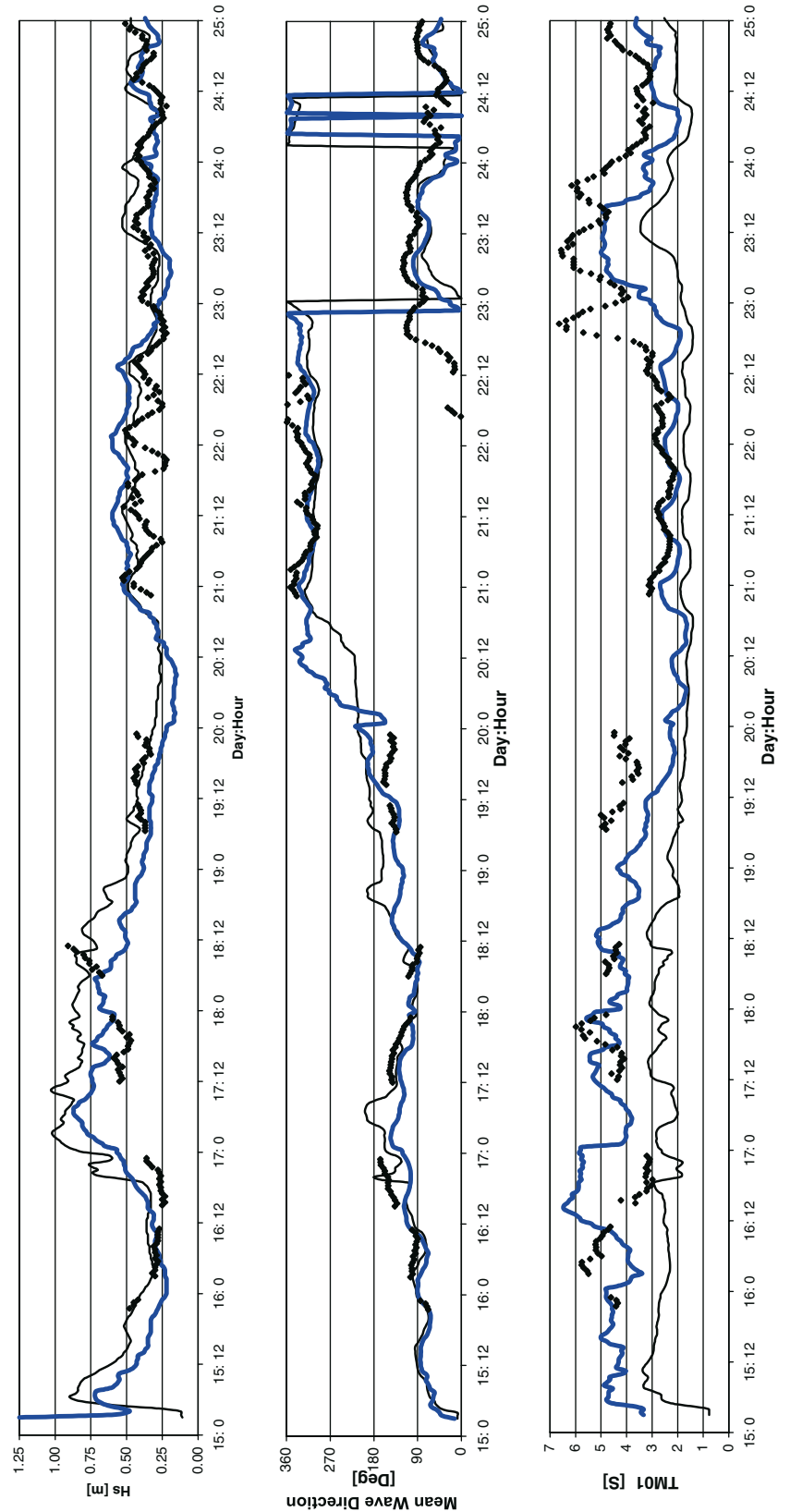
**Fig. 9** Time series of integrated parameters at Westerland for the selected simulation period in November 2002. *Top panel* significant wave heights, *second panel* mean wave direction ('going to'), *lower panel*  $T_{m01}$  period. *Thick lines* K-model results, *thin lines* SWAN results, *stars* buoy measurements. Models results include tidal effects



at the western and northern boundaries. Three-hourly data was extracted from results of the WAM cyc4 model from the HIPOCAS project (grid resolution:  $\sim 5.6$  km) at 43 points, as close as possible to the open boundary of

our coarse grid. Regarding different philosophies of numerical integration of the action density equation and using different independent variables, boundary spectra had to be transferred to proper variables and formats for

**Fig. 10** Time series of integrated parameters at Hoernum for the selected simulation period in November 2002. *Top panel* significant wave heights, *second panel* mean wave direction ('going to'), *lower panel*  $T_{m01}$  period. *Thick lines* K-model results, *thin lines* SWAN results, *stars* buoy measurements. Models results include tidal effects



both the SWAN and K-model. A good quality of the WAM boundary spectra could be verified by comparing significant wave heights at three locations on a cross-section from the open boundary to the Westerland buoy

location. At the buoy location ( $\sim 3$  km off-shore) and during the simulation period of mainly on-shore blowing winds, WAM results are in the order of those of the other models and agree quite well with measurements.

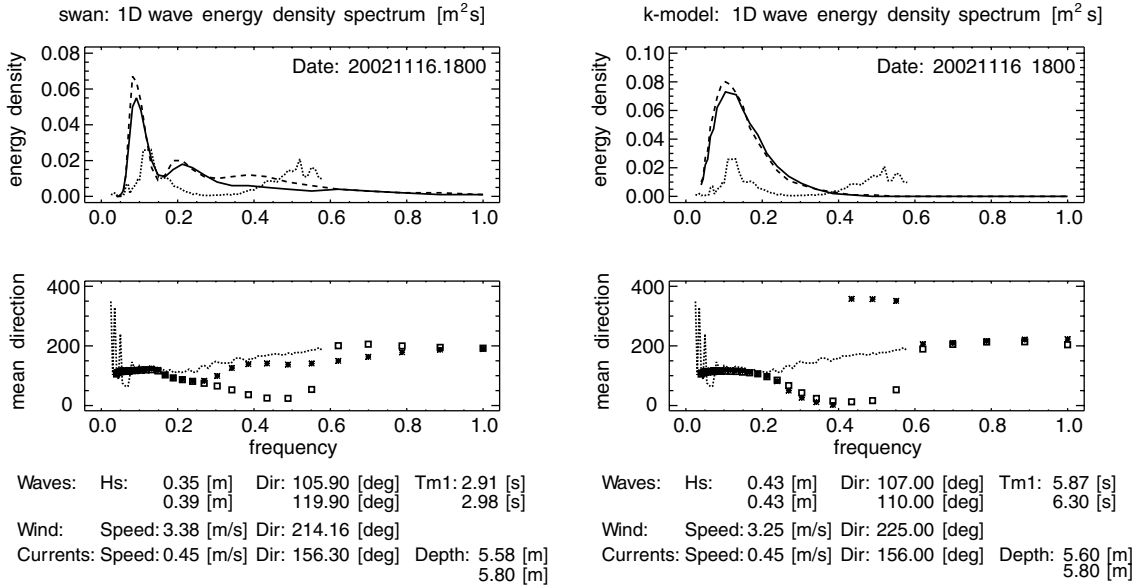
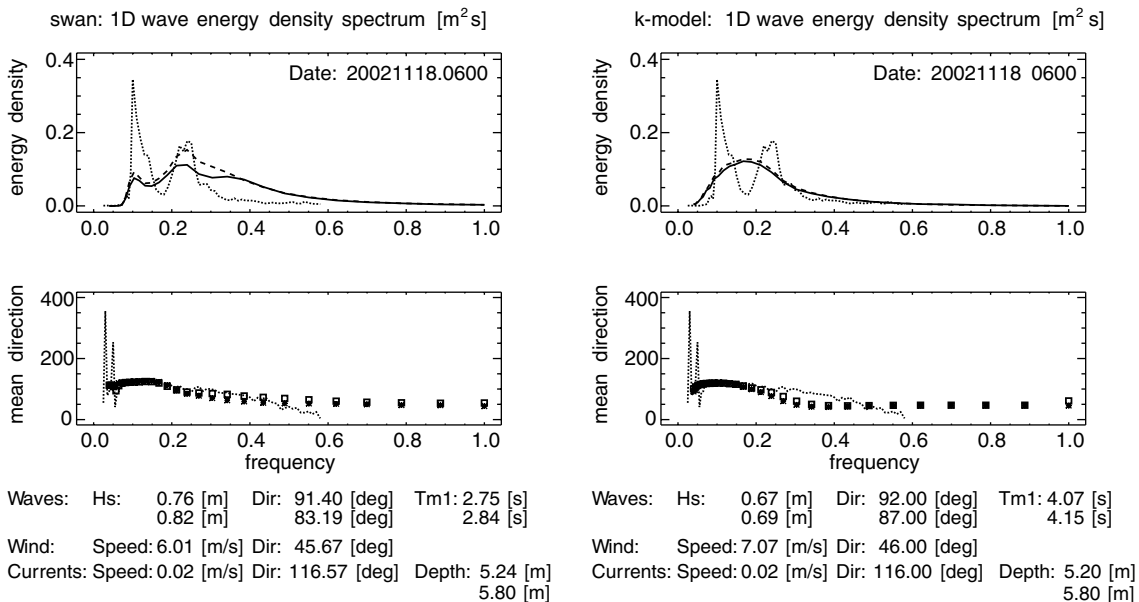


**Fig. 11** 1D-spectra at Hoernum at 16th of November 18:00 h. Dotted lines measured, thick lines modeled (dashed and stars no tides, solid and squares with tides). Left panels SWAN, right panels K-model. Integrated parameters: first line tides included; second line no tides

### 3.5 Model resolutions

Both models were running on the same computational grids, namely a  $71 \times 155$  coarse grid with a spatial resolution of 1,600 m and a  $161 \times 81$  nested fine grid with a resolution of 400 m. The spectral resolution was 24 directional bins of  $15^\circ$  and 28 frequency bins between

**Fig. 12** 1D-spectra at Hoernum at 18th of November 06:00 h. Dotted lines measured, thick lines modeled (dashed and stars no tides, solid and squares with tides). Left panels SWAN, right panels K-model. Integrated parameters: first line tides included; second line no tides



0.04 Hz and 1 Hz (SWAN) or wave number bins between  $0.01 \text{ m}^{-1}$  and  $3.33 \text{ m}^{-1}$  (K-model), in order to cover a wide range of possible wave lengths. For output, the wave number spectra of the K-model were transformed to frequency spectra using the same axis as SWAN.

Due to different numerical methods the integration time steps for propagation, refraction, and source terms were chosen in a different way. The integration time steps of 300 s (coarse grid) and 60 s (fine grid) in SWAN are used throughout the simulations. The time steps for propagation, refraction and source term integration can be chosen differently inside the K-model. The propagation time steps were chosen as 30 s (coarse grid) and 10 s (fine grid). With respect to CPU time both models performed comparably, using one of an AMD 2.8 GHz dual processor PC (i.e., 3 days for the fine grid runs for a

**Table 1** Statistical properties of integrated parameters at stations Westerland and Hoernum

Location	Measurements			Models						
	Mean (m or s)	Data points	SD (m or s)	Model	Tidal input	Mean (m or s)	SD (m or s)	SI	Bias (m or s)	RMSE (m or s)
Statistics of significant wave heights $H_s$										
Westerland (depth 13.2 m)	0.513	120	0.144	K-model	Yes	0.492	0.146	0.2850	-0.02	0.1469
					No	0.483	0.147	0.2859	-0.03	0.1489
				SWAN	Yes	0.666	0.164	0.3199	0.154	0.2243
					No	0.652	0.157	0.3068	0.139	0.2094
Hoernum (depth 5.8 m)	0.389	301	0.117	K-model	Yes	0.413	0.135	0.3477	0.024	0.1372
					No	0.417	0.150	0.3854	0.028	0.1524
				SWAN	Yes	0.465	0.113	0.2897	0.076	0.1359
					No	0.476	0.123	0.3158	0.086	0.1504
Statistics of $T_{m01}$ period										
Westerland (depth 13.2 m)	3.843	120	0.882	K-model	Yes	3.710	0.999	0.2599	-0.133	1.0037
					No	3.811	1.034	0.2692	-0.032	1.0306
				SWAN	Yes	2.441	0.741	0.1928	-1.402	1.5842
					No	2.572	0.658	0.1712	-1.271	1.4303
Hoernum (depth 5.8 m)	4.010	301	1.173	K-model	Yes	3.360	1.201	0.2995	-0.650	1.3642
					No	3.484	1.216	0.3032	-0.527	1.3232
				SWAN	Yes	2.085	0.995	0.2481	-1.926	2.1669
					No	2.253	1.004	0.2504	-1.758	2.0236

*SD* Standard deviation, *RMSE* root mean square error, *SI* scatter index

10-day simulation period). To reduce the computational time considerably, SWAN could also be used in a quasi-steady approach with multiple stationary computations. It was beyond the scope of this work (but will be done later) to use this feature of SWAN and to examine possible differences compared to the results presented here.

## 4 Results

### 4.1 Available wave measurements

K-model and SWAN computations for the 10-day period in November 2002 were compared with data measured by directional wave rider buoys, one located approximately 3 km off-shore from Westerland/Sylt at a water depth of 13.2 m, another north of the Hoernum tidal inlet and approximately 1 km off the coast of Sylt at a water depth of 5.8 m (see Fig. 6). The Westerland buoy data were available at 2-h intervals, and Hoernum buoy data were accessible every 0.5 h. Processed spectra consisted of 64 energy densities in the frequency range between 0.025 Hz and 0.580 Hz. No tail-correction above the cut-off frequency was performed.

### 4.2 Model comparison

The primary objective of the November 2002 hindcast experiment was the comparison of K-model and SWAN results with the field data. Hereafter, results of model runs with and without tidal water level and current

variations will be discussed. All directions are defined as “going to” referring to the clockwise system  $0^\circ$  pointing to the North,  $90^\circ$  to the East,  $180^\circ$  to the South and  $270^\circ$  to the West. Integration of the modeled  $T_{m01}$  periods was performed over the whole frequency range between 0.04 Hz and 1 Hz.

Time series of integrated wave parameters (from measurements and model runs including water level and current variations) are given in Figs. 9 (Westerland) and 10 (Hoernum) for the period, 15th to 25th of November 2002.

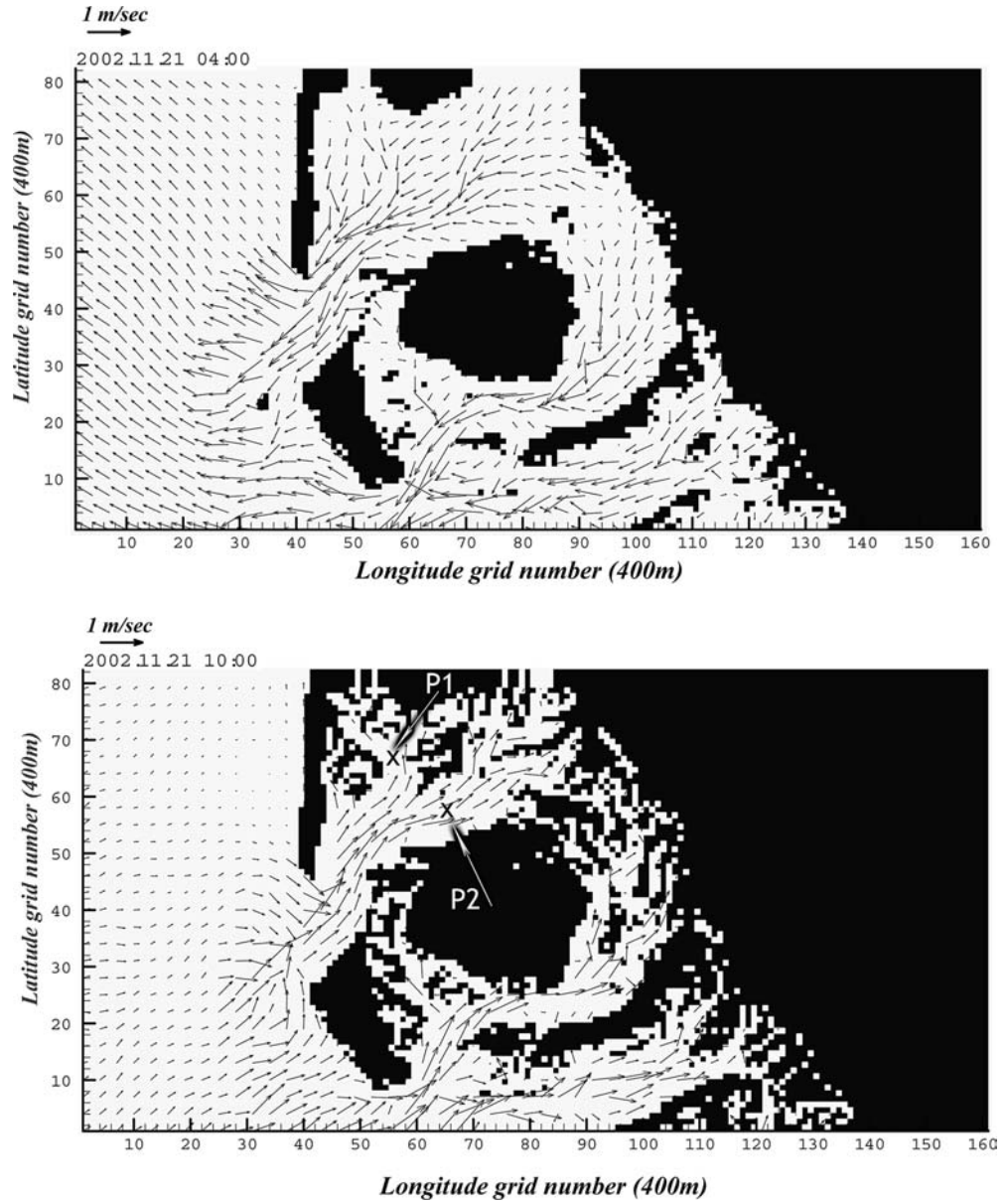
Wind measurements and model input data at Westerland (Fig. 7) show a fairly low wind speed period during the first 5 days of the simulation. Mean wave directions during this period are mainly directed on-shore (Figs. 9, 10, second panel). After 20th of November wind direction changed to the West and wave heights (upper panel) are generally fetch-limited. After 22nd of November mean wave directions changed again to easterly directions. This directional change is in accordance with the observed increase of  $T_{m01}$  periods (lower panel).

Significant wave height ( $H_s$ ) results from both the K-model and SWAN agree fairly well with wave rider measurements. K-model  $T_{m01}$  periods match better to the measurements than SWAN periods which show very little variations.

Greater differences are observed at certain times. In the following, we selected a few situations to indicate model limitations or problems with measurements.

At both stations, especially at Hoernum, measured significant wave heights show greater oscillations during the 21st and 22nd of November 2002 than the models results. This may be due to the positions and mooring of

**Fig. 13** Modeled current fields; *upper panel* ebb flow at 21st of November 04:00 h, *lower panel* flood at 21st of November 10:00 h. Vector lengths are proportional to velocities



the buoys in an environment where high speed currents occur, causing large horizontal displacements and tilting of the buoys. As the buoys try to adjust to their initial horizontal orientation, this additional acceleration may be misinterpreted as a change in wave height. This malfunctioning is pronounced at a frequency of 0.06 Hz, where a sharp peak appears (see for example upper spectrum in Fig. 16). In the calculation of the measured integrated parameters these peaks were omitted.

In cases when initially two peaked spectra travel in an on-shore direction, SWAN keeps the spectral form, whereas the K-model dissipates the energies contained in the second peak during propagation. This can be seen in the 1D spectral plots of Fig. 11 for 16th of November, hour 18:00.

On the 18th of November two wave systems arrive from the West as can be seen in the spectral plots in

Fig. 12. K-model results show only one-peaked spectrum, corresponding to the input spectra at the western boundary. Due to nonlinear interaction SWAN may have generated a two peak spectrum, a behavior we already noticed in the artificial test cases.

The overall statistics for the comparisons of modeled and measured significant wave heights and  $T_{m01}$  periods, with and without tidal input are presented in Table 1. Wave modeling results of the simulation period from 15th of November to 25th of November 2002 have been used for the statistical analysis at the two buoy stations Westerland and Hoernum.

The analysis shows that the statistical parameters for  $H_s$  are very similar, whether or not tidal variations are taken into account, a result we already expected from the comparison of the time series. Biases of both models are rather small and in the order of a few centimeters.

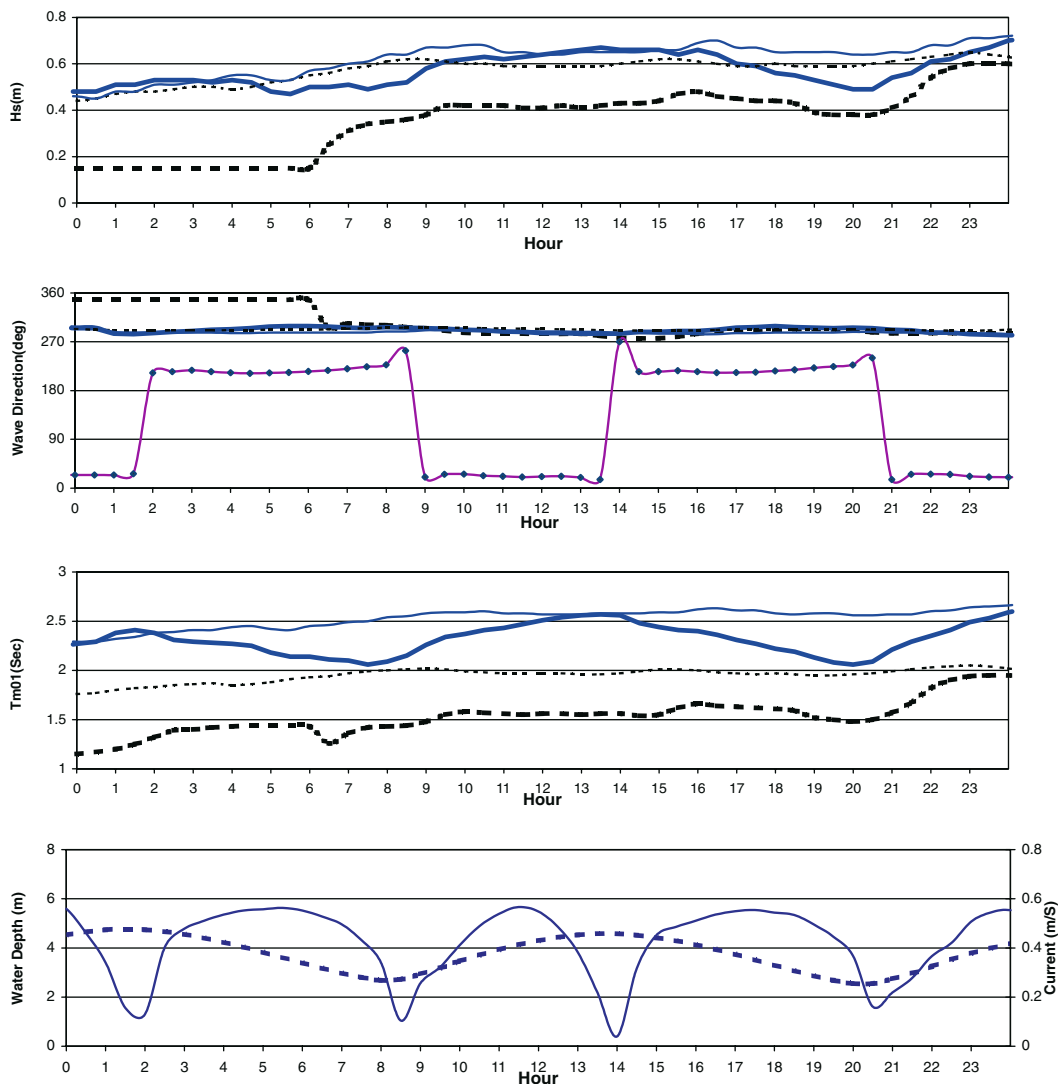


**Fig. 14** Time series of integrated parameters and tidal input data for 21st of November at P1 (see Fig. 13 for location) with (*thick lines*) and without (*thin lines*) tidal input. *Dashed lines* SWAN, *continuous lines* K-model, *thin line with stars* in second panel current direction. *Bottom panel* current speed (*full line*) and water depth variation (*dashed line*)

levels, and by integration leads to lower periods with low variability during time. Although the standard deviations and scatter indices of the SWAN results are generally better than those of the K-model the RMSE errors are not. Both models show rather high errors in the order of 1–2 s.

SWAN overestimates a little bit. At Hoernum, the root mean square errors (RMSE) of both the K-model and SWAN are in the order of 14–15 cm. At Westerland, the RMSE errors of SWAN are 7 cm higher than the error of 15 cm for the K-model. Scatter indices are in the order of 30%.

Especially for the Westerland buoy location with a depth of 13.2 m and approximately 3 km off-shore, an obvious change of  $T_{m01}$  due to Doppler shift effects is not expected. This effect vanishes, mainly because waves are propagating more or less perpendicular to the coastal current.

At both stations, K-model shows less  $T_{m01}$  biases than SWAN. This is due to the double-peak spectra of SWAN, the peaks often times at comparable energy

### 4.3 Effects of currents on wave fields

To indicate various effects of currents and water depth variations on modeled wave parameters in more detail, time series of integrated wave parameters and tidal properties at two different points (see Fig. 13) inside the tidal basin are presented in Figs. 14 and 15 for 21st of November 2002. During this day the off-shore wind is steadily directed to about  $285^\circ$  generating fetch-dependent wind waves. Snapshots of the current field (Fig. 13) on 21st of November 2002 at 04:00 h represent ebb condition and at 10:00 h represent flood condition, respectively.

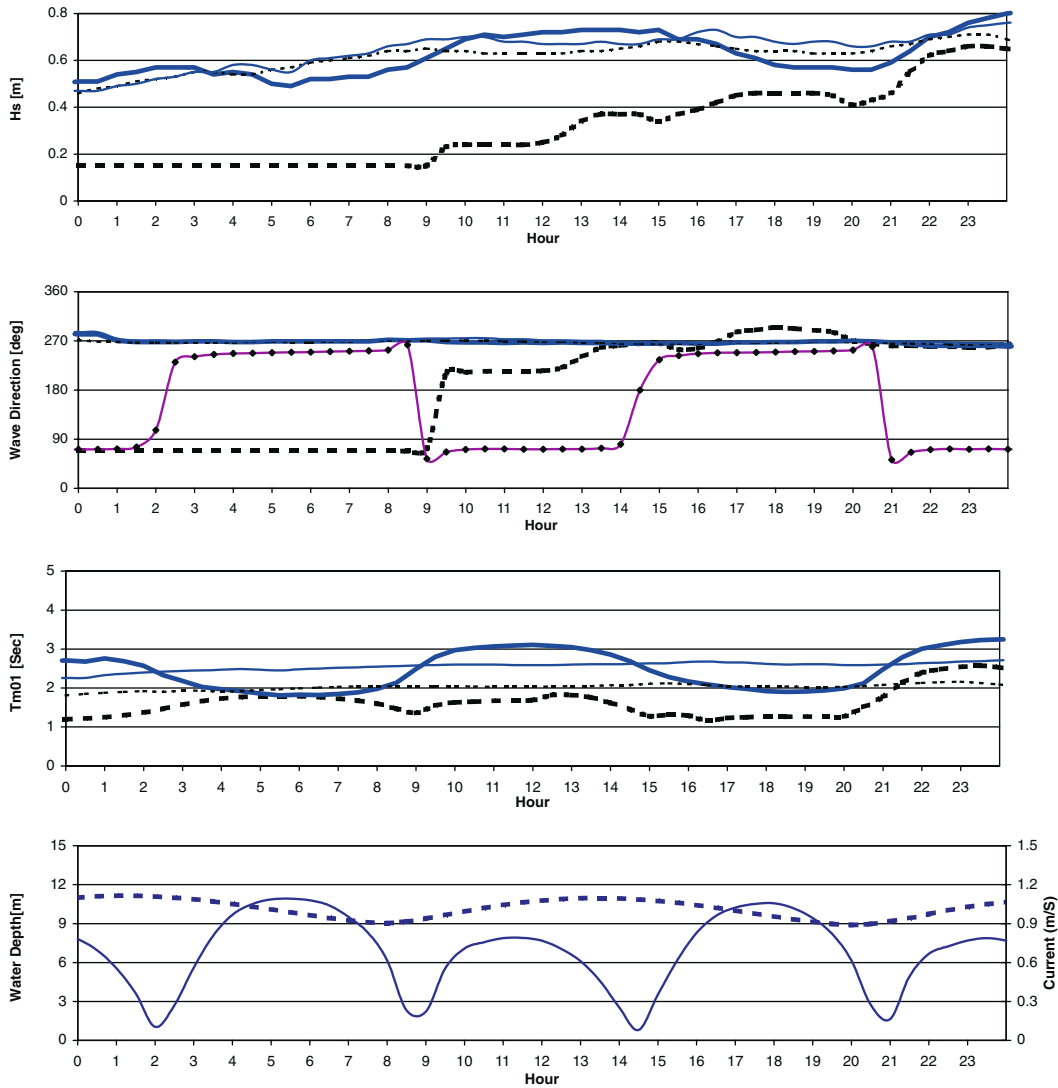


**Fig. 15** Time series of integrated parameters and tidal input data for 21st of November at P2 (see Fig. 13 for location) with (*thick lines*) and without (*thin lines*) tidal input. *Dashed lines* SWAN, *continuous lines* K-model, *thin line with stars in second panel* current direction. *Bottom panel* current speed (*full line*) and water depth variation (*dashed line*)

At point P1 (Fig. 14) located in the northern channel, current directions switch between  $20^\circ$  at ebb tide and  $200^\circ$  during flood, in both cases more or less perpendicular to the mean wave direction. Thus, any changes in  $H_s$  and  $T_{m01}$  are not due to Doppler shift effects but to water depth variations. This is visible in the K-model results. The wave heights and periods decrease during low tides.

SWAN model results change considerably, when tidal water level variations and currents are included. Linear wind wave growth was not activated in both the cases and thus can't explain the drop in significant wave height. Inclusion of linear wind wave growth would have increased the energy level due to stronger up-wind wave generation at initial states.

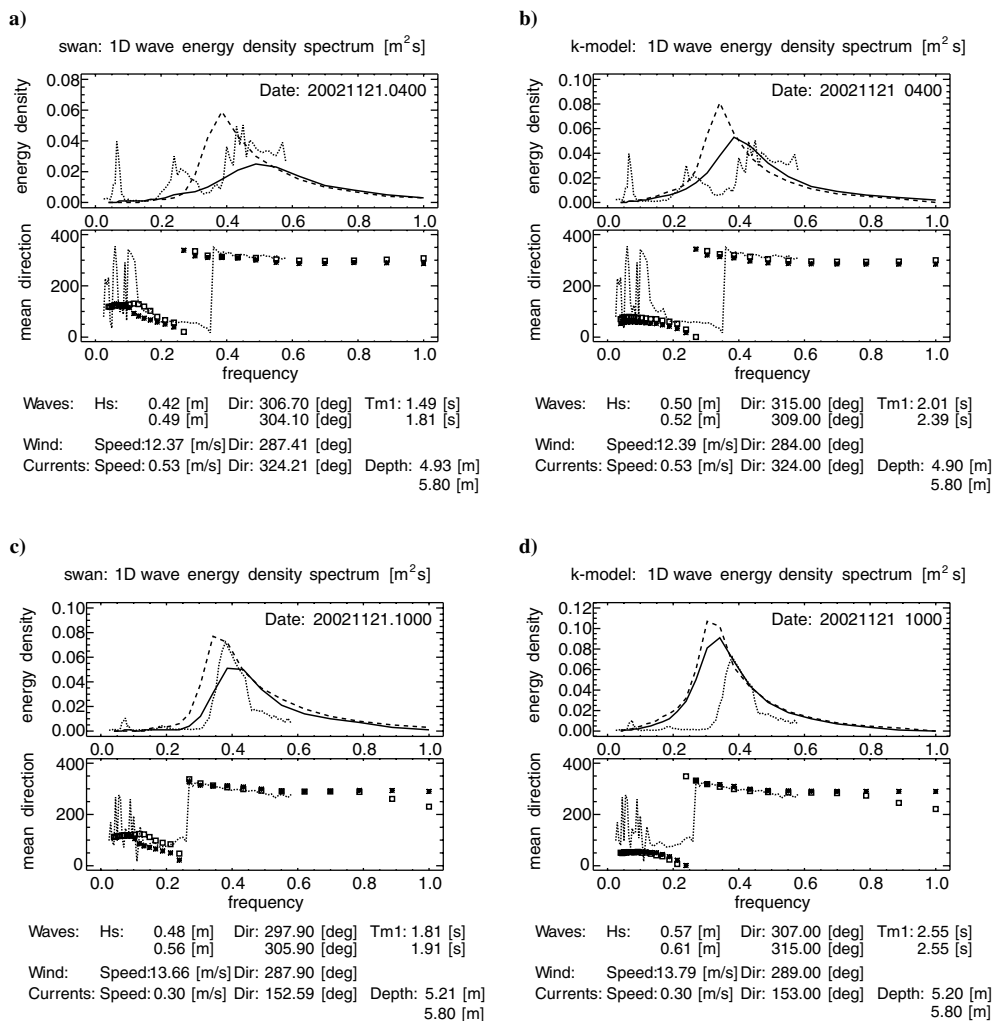
Output results of both models for point P2 are presented in Fig. 15. At this location we observe following currents during ebb condition and opposing currents at flood times. Taking currents into account, the  $T_{m01}$  period calculated by the K-model is changed by approximately  $-0.5$  s (ebb) and  $0.5$  s (flood). Those changes are in agreement with simplified calculations using the dispersion and Doppler-shift relation (Eqs. 1 and 2). In case of the SWAN model, taking currents into account decreases the period most of the times, regardless of ebb or flood conditions.

Similar to the results at P1, significant wave heights of SWAN show very low values in cases in which tides are included.

Some general features can be examined with the help of maps (not shown here) of  $H_s$  and  $T_{m01}$  model results (with and without tides). During ebb condition at 04:00 h we observe:

1. Wave heights in inner parts of the basin are strongly depth dependent;
2. Fetch limited wave growth is visible;

**Fig. 16** Measured (*dotted lines*) and modeled 1D-spectra (*dashed and stars no tides, solid and squares with tides*) at Hoernum for the 21st of November 04:00 h (*upper panels*) and 10:00 h (*lower panels*). *Left panels* SWAN, *right panels* K-model. Integrated parameters: *first line* tides included; *second line* no tides



- SWAN generally generates lower  $T_{m01}$  periods than K-model;
- Where current and wind wave directions are similar, which is especially the case at the tidal inlet, the effect of following currents is detectable as a decreasing  $H_s$  and  $Tm01$ .

Maps from 10:00 h characterize the wave climate during flood:

- Lower wave heights in those parts of the basin with still lower water;
- In the northern part of the tidal inlet and in the main channels where opposing currents with speeds of 0.6–1.0 m/s occur, an increase of up to 1 s in  $T_{m01}$  is observed.

For both dates, the impact of currents on waves is examined further by looking at 1D wave spectra at the Hoernum buoy location (Fig. 16).

At 04:00 h we have a current with a speed of 0.53 m/s and a direction of 324° and mean wave directions of about 310°. A shifting of wave energy densities to higher frequencies is expected when currents are included. This is obvious in Fig. 16a, b (upper panels), also show a

much better agreement with the measured 1D-spectrum. Mean directions are also in a good agreement. Integrations lead to a K-model wave height of  $H_s=0.50$  m and a SWAN wave height of  $H_s=0.42$  m, which compares very well with the measured  $H_s=0.40$  m.

The peak frequencies of the K-model are generally lower than those of SWAN leading to higher  $T_{m01}$  periods.

At 10:00 h (flood condition, opposing current) the peak frequency of the K-model in both cases (with and without currents) stays at a low value of about 0.3 Hz (Fig. 16, panel d). SWAN spectra show a shift from approximately 0.32 Hz to 0.4 Hz (Fig. 16, panel c), both spectra are comparable with the measured spectrum than those of the K-model with respect to energy levels and positions. Mean directions of modeling results and measurements are in a good agreement.

## 5 Summary and conclusion

The motivation of this work was primarily to carry out a comprehensive study of two third generation wave models in a real shallow water application, and to clarify



the influence of different source terms on the results in artificial test cases.

SWAN and K-model differ in their numerical and physical approaches, giving advantage to one or the other in different situations. K-model's concept of nonlinear dissipation seems to work with respect to the significant wave height parameter. Inclusion of triad interaction enables SWAN to produce second harmonics in an initially one peaked spectrum which are also observed at measurement stations in shoaling waters.

During the 10 days hindcast of the German Bight application, there were periods with westerly winds at moderate speeds leading to interesting wave systems of old and young wind seas. During the second half of the simulation period easterly winds prevailed with speeds of up to 15 m/s, generating fetch limited sea states inside the Hoernum Bight and off the coast of Sylt.

It is taken into account that tides can change the results considerably, especially in areas where high current velocities and large water depth variations occur. Spectral shapes are improved; in particular peak frequencies are adjusted to observed values due to Doppler shift effects. In this respect, SWAN performed better than the K-model, especially when the measurements showed two peaks, but energies were often at a lower level compared to those of K-model and measurements. Due to comparable energy levels of the two peaks of SWAN spectra,  $T_{m01}$  periods of SWAN were too low with hardly any variability throughout the 10-day simulation period in November 2002.

Both models followed the measured significant wave heights; however SWAN overestimated, leading to a bias of up to +15 cm.

**Acknowledgements** The authors are indebted to Dr. Wolfgang Rosenthal for many clarifying discussions, and Dr. Harmut Kapitza, Dr. Dieter Eppel and Dr. Walter Puls for their support by providing the hydrodynamical model, bathymetry and boundary data. The authors would also like to thank Dr. Marcel Zijlema of the SWAN group at Delft University of Technology, for his assistance. This work was performed as part of a Ph.D. program supported by the Iranian Ministry of science, research and technology and the GKSS Research Center, Geesthacht, Germany. Corresponding financial and scientific support is gratefully acknowledged.

## References

- Arcilla AS, Roelvink JA, O'Conner BA, Reniers A, Jimenez JA (1994) The Delta Flume '93 experiment. *Coastal Dynamics 1994*, ASCE, pp 488–502
- Battjes JA, Janssen JPFM (1978) Energy loss and set-up due to breaking of random waves. In: *Proceeding of 16th international conference on coastal engineering*, ASCE, pp 569–587
- Booij N, Ris RC, Holthuijsen LH (1999) A third-generation wave model for coastal regions. 1. Model description and validation. *J Geophys Res* 104(C4):7649–7666
- Casulli V, Cattani E (1994) Stability, accuracy and efficiency of a semi-implicit method for three-dimensional shallow water flow. *Comput Math Appl* 27:99–112
- Casulli V, Cheng RT (1992) Semi-implicit finite difference methods for three dimensional shallow water flow. *Int J Numer Methods Fluids* 15:629–648
- Cavaleri L, Rizzoli PM (198) Wind wave prediction in shallow water—theory and application. *J Geophys Res* 86:10961–10973
- Eldeberky Y (1996) Nonlinear transformation of wave spectra in the nearshore zone. PhD Thesis, Delft University of Technology, Department of Civil Engineering, The Netherlands
- Eldeberky Y, Battjes JA (1995) Parameterization of triad interactions in wave energy models. In: *Proceedings of coastal dynamics conference'95*, Gdansk, pp 140–148
- Eppel DP, Kapitza H, Onken R, Pleskatchevski A, Puls W, Rietmueller R, Vaessen B (2003) BELAWATT-Watthydrodynamik: Die hydrodynamische Belastung von Wattgebieten. GKSS Research Center Publication, Germany
- Günther H, Rosenthal W (1995) A wave model with a non-linear dissipation source function. In: *Proceedings of the 4th international workshop on wave hindcasting and forecasting*, Banff
- Günther H, Hasselmann S, Janssen PAEM (1992) The WAM Model cycle-4.0. User manual. Deutsches Klimarechenzentrum Hamburg, Technical Report No. 4
- Hasselmann K, Barnett TP, Bouws E, Carlson H, Cartwright DE, Enke K, Ewing JA, Gienapp H, Hasselmann DE, Krusemann P, Meerburg A, Müller P, Olbers DJ, Richter K, Sell W, Walden H (1973) Measurements of wind-wave growth and swell decay during the Joint North Sea Wave Project (JONSWAP). *Deutsche Hydrographische Zeitschrift Suppl* A8(12):95
- Hasselmann S, Hasselmann K, Allender JH, Barnett TP (1985) Computations and parameterizations of the nonlinear energy transfer in a gravity wave spectrum. Part II: parameterizations of the nonlinear transfer for application in wave models. *J Phys Oceanogr* 15(11):1378–1391
- Holthuijsen LH, Booij N, Ris RC, Haagsma IJG, Kieftenburg ATMM, Kriezi EE, Zijlema M, van der Westhuysen AJ (2004) SWAN Cycle III Version 40.31 User Manual. Delft University of Technology, The Netherlands.
- Komen GJ, Cavaleri L, Donelan M, Hasselmann K, Hasselmann S, Janssen PAEM (1994) *Dynamics and Modelling of Ocean Waves*. Cambridge University Press, London
- Lin W, Sanford LP, Suttles SE (2002) Wave measurement and modeling in Chesapeake Bay. *Cont Shelf Res* 22:2673–2686
- Luo W, Sclavo M (1997) Improvement of the third generation WAM model (cycle-4) for applications in the near shore regions. Proudman Oceanographic Laboratory. Internal document No. 116
- Monbaliu J, Padilla-Hernandez R, Hargreaves JC, Albiach JCC, Luo W, Sclavo M, Günther H (2000) The spectral wave model, WAM, adapted for applications with high spatial resolution. *Coast Eng* 41:41–62
- Ris RC, Holthuijsen LH, Booij N (1999) A third-generation wave model for coastal regions. 2.Verification. *J Geophys Res* 104(C4):7667–7681
- Rosenthal W (1989) Derivation of Phillips  $\alpha$ -parameter from turbulent diffusion as a damping mechanism. In: Komen GJ, Oost WA (eds) *Radar Scattering from Modulated Wind Waves*. Kluwer, Dordrecht, pp 81–88
- Schneggenburger C, Günther H, Rosenthal W (1997) Shallow water wave modelling with nonlinear dissipation. *Deutsche Hydrographische Zeitschrift* 49:431–444
- Schneggenburger C, Günther H, Rosenthal W (2000) Spectral wave modelling with non-linear dissipation: validation and applications in a coastal tidal environment. *Coast Eng* 41:201–235
- Tolman HL (1991) A third-generation model for wind waves on slowly varying, unsteady and inhomogeneous depths and currents. *J Phys Oceanogr* 21:782–797
- Tolman HL, Chalikov DV (1996) Source terms in a third-generation wind wave model. *J Phys Oceanogr* 26:2497–2518
- WAMDI Group, Hasselmann S, Hasselmann K, Bauer E, Janssen PAEM, Komen GJ, Bertotti L, Lionello P, Guillaume A, Cardone VC, Greenwood JA, Reistad M, Yambresky L, Ewing JA (1988) The WAM model—a third generation ocean wave prediction model. *J Geophys Res* 18:1775–1810

- Weisse R, Gayer G (2000) An approach towards a 40-year high-resolution wave hindcast for the Southern North Sea. In: Proceedings of 6th international workshop on wave hindcasting and forecasting, Monterey, pp 6–10
- Wornom SF, Welsh DJS, Bedford KW (2001) On coupling of SWAN and WAM wave models for accurate nearshore wave predictions. *Coast Eng J* 43(3):161–201
- Wornom SF, Welsh DJS, Bedford KW (2002) The effect of wave propagation scheme on nearshore wave predictions. *Coast Eng J* 44 (4):359–371